

Magnetoelectric and multiferroic properties of variously oriented epitaxial BiFeO₃ – CoFe₂O₄ nanostructured thin films

Li Yan, Zhiguang Wang, Zengping Xing, Jiefang Li, and D. Viehland

Citation: *Journal of Applied Physics* **107**, 064106 (2010); doi: 10.1063/1.3359650

View online: <http://dx.doi.org/10.1063/1.3359650>

View Table of Contents: <http://scitation.aip.org/content/aip/journal/jap/107/6?ver=pdfcov>

Published by the AIP Publishing

Articles you may be interested in

Multiferroic and magnetoelectric properties of CoFe₂O₄/Pb_{1-x}Sr_xTiO₃ composite films

J. Appl. Phys. **117**, 164101 (2015); 10.1063/1.4918663

Adjustable magnetoelectric effect of self-assembled vertical multiferroic nanocomposite films by the in-plane misfit strain and ferromagnetic volume fraction

J. Appl. Phys. **115**, 114105 (2014); 10.1063/1.4868896

Local probing of magnetoelectric coupling and magnetoelastic control of switching in BiFeO₃-CoFe₂O₄ thin-film nanocomposite

Appl. Phys. Lett. **103**, 042906 (2013); 10.1063/1.4816793

Influence of relative thickness on multiferroic properties of bilayered Pb (Zr_{0.52}Ti_{0.48})O₃ – CoFe₂O₄ thin films

J. Appl. Phys. **104**, 114114 (2008); 10.1063/1.3035851

Orientation-dependent multiferroic properties in Pb (Zr_{0.52}Ti_{0.48})O₃ – CoFe₂O₄ nanocomposite thin films derived by a sol-gel processing

J. Appl. Phys. **103**, 034103 (2008); 10.1063/1.2838482

MIT LINCOLN
LABORATORY
CAREERS

Discover the satisfaction of
innovation and service
to the nation

- Space Control
- Air & Missile Defense
- Communications Systems & Cyber Security
- Intelligence, Surveillance and Reconnaissance Systems
- Advanced Electronics
- Tactical Systems
- Homeland Protection
- Air Traffic Control


LINCOLN LABORATORY
MASSACHUSETTS INSTITUTE OF TECHNOLOGY



LEARN MORE

Magnetoelectric and multiferroic properties of variously oriented epitaxial BiFeO₃–CoFe₂O₄ nanostructured thin films

Li Yan,^{a)} Zhiguang Wang, Zengping Xing, Jiefang Li, and D. Viehland

Department of Materials Science and Engineering, Virginia Tech, Blacksburg, Virginia 24061, USA

(Received 3 December 2009; accepted 6 February 2010; published online 30 March 2010)

We report the ferroelectric, ferromagnetic, and magnetoelectric (ME) properties of self-assembled epitaxial BiFeO₃–CoFe₂O₄ (BFO–CFO) nanostructure composite thin films deposited on (001), (110), and (111) SrTiO₃ (STO) single crystal substrates. These various properties are shown to depend on orientation. The maximum values of the relative dielectric constant, saturation polarization, longitudinal piezoelectric coefficient, saturation magnetization, and ME coefficient at room temperature were 143, 86 $\mu\text{m}/\text{cm}^2$, 50 pm/V, 400 emu/cc, and 20 mV/cm Oe, respectively.

© 2010 American Institute of Physics. [doi:10.1063/1.3359650]

I. INTRODUCTION

Magnetoelectric (ME) materials exhibit an induced polarization under external magnetic field H , or an induced magnetization under external electric field E . The concept of magnetoelectricity was originally proposed by Curie in 1894.¹ It was first experimentally found in the single phase material Cr₂O₃, where the H -induced polarization and E -induced magnetization were reported by Astrov in 1960^{2,3} and Rado *et al.*⁴ in 1961. Compared with single phase multiferroic materials, composite multiferroics have higher ME effects.^{5–10} Through a stricitive interaction between the piezoelectricity of the ferroelectric (FE) phase and the magnetostriction of the ferromagnetic (FM) phase, said composites are capable of producing relatively large ME coefficients.

The most widely studied phase connectivities for two-phase ME composite films are (i) a (2–2) layer-by-layer structure^{11–18} and (ii) a (0–3) structure of second phase particles embedded in a primary matrix phase.^{19,12,20–23} In addition, (1–3) self-assembled ME composite thin films consisting of FE [or (FM)] nanopillars embedded in a FM (or FE) matrix was first reported in 2004.²⁴ Self-assembled epitaxial BiFeO₃–CoFe₂O₄ (BFO–CFO) nanocomposite thin films deposited on differently oriented substrates are known to have different types of nanostructures.²⁵ On (001) SrTiO₃ (STO) substrates, BFO pyramidal nanopillars are embedded in a CFO matrix, on (111) STO, CFO triangular nanopillars are embedded in a BFO matrix, and on (110) CFO, a nanoridge is embedded in a BFO matrix. Which phase spreads as the matrix versus which one is spatially confined to become nanopillars depends on wetting conditions between film and substrate, for example, CFO wets well on (111) STO but not on (001).²⁶ Although it was predicted that (1–3) self-assembled multiferroic composite thin films should have better ME coupling because of reduced constraint between nanopillars and substrate,²⁷ it is difficult to deposit such nanostructures with satisfactory FE properties. Accordingly, reports of multiferroic properties of self-assembled nano-

composites are quite limited, in particular compared with layer-by-layer and particle-matrix composite structures.

Here, we report the FE, FM, and ME properties of self-assembled epitaxial BFO–CFO nanocomposite thin films deposited on variously oriented substrates. It was found that the FE and FM properties of the nanocomposites are strongly related to the orientations of the BFO phase and the nanostructure of the CFO phase, respectively, whereas the ME properties depend not only on the FE and FM properties of each individual phase, but also on how the nanostructures couples them together.

II. EXPERIMENTAL PROCEDURE

Two phase 0.65BiFeO₃–0.35CoFe₂O₄ epitaxial thin films were deposited by pulsed laser deposition on (001), (110), and (111) oriented SrTiO₃ (STO) substrates, both with and without SrRuO₃ (SRO) bottom electrodes for FE and FM measurements, respectively. The thickness of the films was varied from 150 to 240 nm, which was measured by scanning electron microscopy. The films were deposited using a Lambda 305i KrF laser with wavelength of 248 nm, focused to a spot size of 2 mm², and incident on the surface of a target using an energy density of 3.0 J/cm². The distance between the substrate and target was 6 cm, and the base vacuum of the chamber was $<10^{-5}$ Torr. The films were deposited at 700 °C with a 90 mTorr oxygen pressure. The surface topology of the BFO–CFO thin films was studied by atomic force microscopy (AFM) (Veeco 3100). The crystal structures of the films were determined using a Philips X'pert high resolution x-ray diffractometer (XRD) equipped with a two bounce hybrid monochromator, and an open three-circle Eulerian cradle. The magnetic properties of the CFO layers were measured at 250 K using a superconducting quantum interference device (SQUID) (Quantum Design MPMS magnetometer), and the ME properties of the nanocomposite films by a magnetic cantilever method.²⁸

III. EPITAXIAL NANOSTRUCTURES

Epitaxy of BFO–CFO films deposited on (001), (110), and (111) STO substrates with SRO buffer layers was con-

^{a)}Electronic mail: liyan@vt.edu.

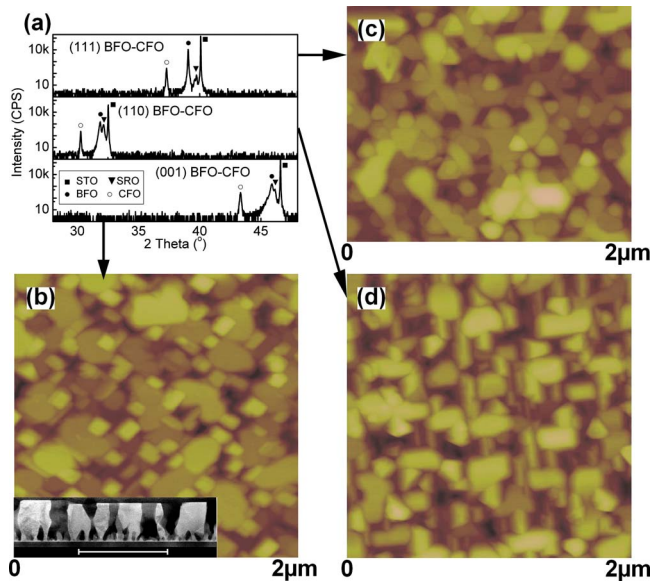


FIG. 1. (Color online) X-ray diffraction line scan and AFM image for (001), (110), and (111) BFO–CFO thin films. (a) XRD line scan over a wide range of angles that demonstrate phase purity and good epitaxy and AFM images that demonstrate the nanostructures of (b) (001), (c) (110), and (d) (111) oriented thin films, where the inset of (b) is cross-section TEM image of (001) BFO–CFO film.

firmed by XRD, as shown in Fig. 1(a). For (001) layers, the peaks between $43^\circ < x < 47^\circ$ were (004) CFO, (002) BFO, (002) SRO, and (002) STO. The (002) of BFO and SRO were very close. For (110) layers, the peaks between $30^\circ < x < 33^\circ$ were (220) CFO, (110) BFO, (110) SRO, and (110) STO. For (111), the peaks between $37^\circ < x < 40^\circ$ were (222) CFO, (111) BFO, (111) SRO, and (111) STO.

The nanostructures of (001), (110), and (111) oriented BFO–CFO layers were studied by AFM, as shown in Figs. 1(b)–1(d), respectively. The nanostructures for these various orientations were similar to that previously reported.²⁵ On (001) STO, the CFO phase formed as pyramidal nanopillars defined by (111) facets and [110] edges, which was embedded in a BFO matrix. On (110) STO, CFO formed as a nanoridge with (111) facet roofs and [110] ridges, embedded in a BFO matrix. On (111) STO, CFO formed as the matrix phase, with embedded BFO triangular nanopillars. The cross-sectional TEM image of the film is shown in the inset of Fig. 1(b), from bottom to top are SrTiO₃, SrRuO₃, and BFO–CFO layers, respectively. The CFO appears as the dark pillars embedded in a bright BFO matrix.

IV. FE PROPERTIES

First, the dielectric properties were studied to ensure that the BFO–CFO nanocomposite films had a relatively high resistance. The room temperature dielectric constants of (001), (110), and (111) BFO–CFO were 143, 97, and 93; and the loss tangents were 0.092, 0.098, and 0.205, respectively. Prior investigations have reported that the dielectric constant of BFO and CFO are 95 and 38,^{29,30} and that the loss tangents are 0.05 and 0.24, respectively. Clearly, our BFO–CFO nanocomposite films have reasonable properties of dielectric insulators.

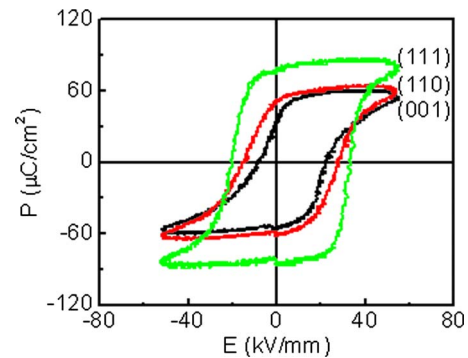


FIG. 2. (Color online) Polarization or P-E hysteresis loops for (111), (110), and (001) BFO–CFO nanocomposite thin films.

The P-E loops for (001), (110), and (111) films were measured at room temperature, as shown in Fig. 2. Polarization saturation is evident in these data, however, some leakage can also be seen at higher electric fields, as evidence by rounding of the corners of the loops. The saturation polarization followed a trend of $P_{s(111)} > P_{s(110)} > P_{s(001)}$ ($86 \mu\text{C}/\text{cm}^2$, $65 \mu\text{C}/\text{cm}^2$, and $60 \mu\text{C}/\text{cm}^2$). The remnant polarization followed a trend of $P_{r(111)} > P_{r(110)} > P_{r(001)}$ ($79 \mu\text{C}/\text{cm}^2$, $55 \mu\text{C}/\text{cm}^2$, and $44 \mu\text{C}/\text{cm}^2$). The coercive fields had a trend of $E_{c(111)} > E_{c(110)} > E_{c(001)}$ (27, 22, and 15 kV/mm).

The longitudinal piezoelectric d_{33} coefficients were then measured by piezoforce microscopy (PFM) as shown in Fig. 3. Maximum values of d_{33} for (001), (110), and (111) BFO–CFO films were determined to be about 50 pm/V, 40 pm/V, and 30 pm/V, respectively. An asymmetry can be seen between the right and left wings for both the (110) and (111) films, where the right side is much lower than the left. Furthermore, the coercive fields for the films were asymmetric. This indicates a built-in field or charge in the thin film, possibly due to defects at the interphase interfaces.

In general, the FE properties of our BFO–CFO nanocomposites were similar to those previously reports for single phase BFO thin films regardless of nanostructure. For example, P_s and E_c for (111) BFO are higher than for the other orientations, both for single phase BFO films³¹ and our BFO–CFO nanocomposite ones. Furthermore, d_{33} was highest for the (001) oriented BFO, both as a single phase layer³¹ and as a BFO–CFO nanocomposite one.

V. FM PROPERTIES

Next, the FM properties were measured at 250 K by SQUID, as shown in Fig. 4. The magnetization values were normalized to the volume fraction of the CFO phase. The shapes of the out-of-plane M-H hysteresis loops of (001), (110), and (111) BFO–CFO were similar to that previously reported for CFO single phase films.^{32–35} This is because the CFO nanostructures for BFO–CFO films along the out-of-plane direction are the same as that for single phase CFO ones, i.e., spin rotation is not limited in the out-of-plane direction. The saturation magnetization was $M_s = 400 \text{ emu/cc}$ and the coercive field was $H_c = 2\text{--}3 \text{ kOe}$. Please note that these values for M_s are a little smaller than those for single phase CFO films, which was reported to be 530 emu/cc .^{32–35}

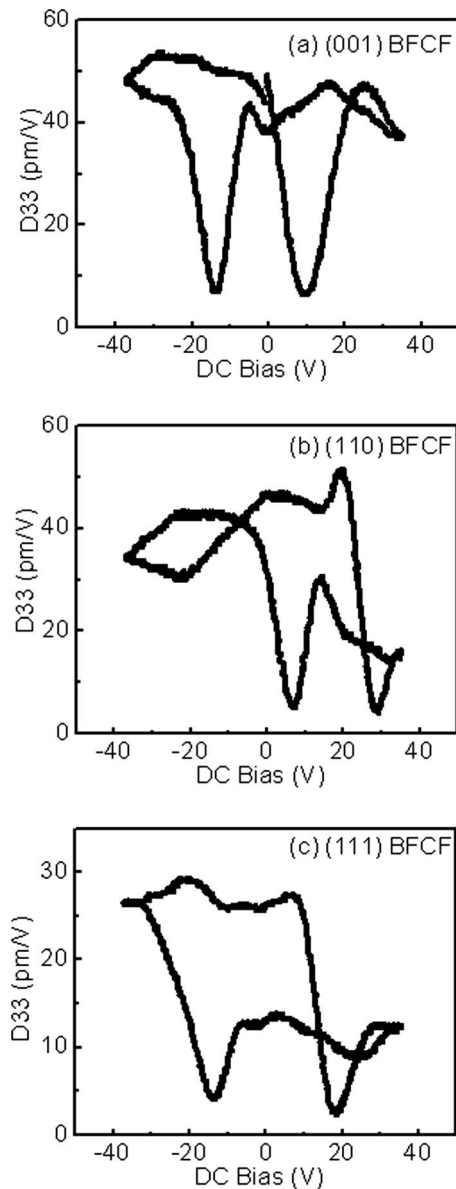


FIG. 3. Longitudinal piezoelectric d_{33} coefficient as a function of dc electric bias for (a) (001), (b) (110), and (c) (111) BFO-CFO nanocomposite thin films.

The M-H loop for the in-plane direction of (001) BFO-CFO is shown in Fig. 4(a). Compared with the out-of-plane loop, the in-plane one has a lower H_c , a lower remnant magnetization M_r , and a higher saturation field (H_s). Because the CFO phase in this case forms as nanopillars embedded in a BFO matrix, the translational symmetry of the CFO phase is broken and the various nanopillars do not connect to each other along the in-plane direction. As a consequence, the spin cannot be stably aligned along the in-plane direction, this makes spin rotation easy but saturation difficult to achieve in-plane.

The M-H loops for the in-plane direction of (111) BFO-CFO were also similar to that previously reported for single phase CFO films,^{32–35} as shown in Fig. 4(c). This is because the CFO phase is the matrix phase, processing dimensional connectivity along the in-plane direction. In addition, the M-H loops for in-plane and out-of-plane directions had simi-

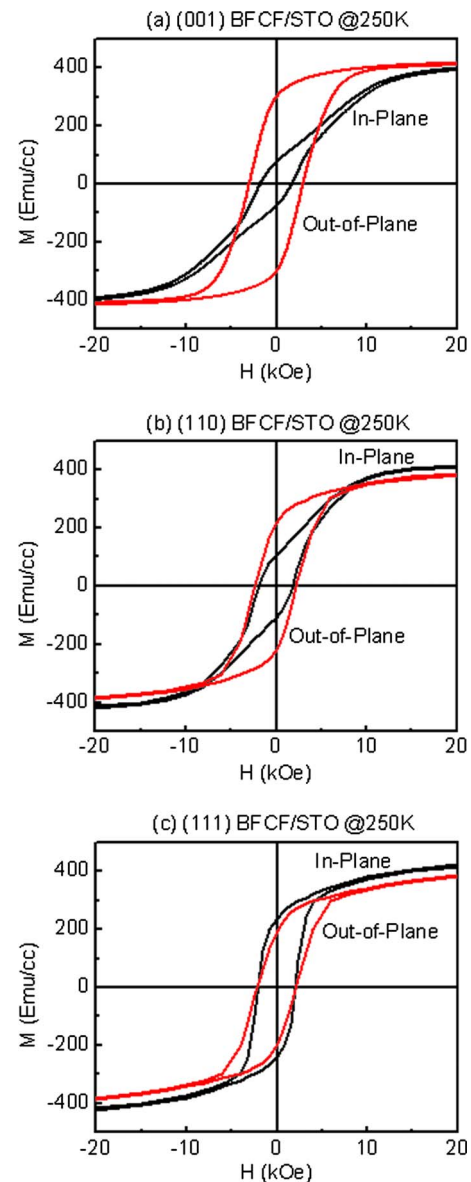


FIG. 4. (Color online) Magnetization or M-H hysteresis loops in both in-plane and out-of-directions for (a) (001), (b) (110), and (c) (111) BFO-CFO nanocomposite thin films. The magnetization was normalized to the volume fraction of the CFO phase.

lar values of H_c and M_r , although M_r in-plane was slightly higher than that out-of-plane, as the spin state is more stable in-plane due to the spread of the CFO matrix phase.

The M-H loops for the in-plane direction of (110) BFO-CFO were intermediate in characteristics between that of (001) and (111) films. The (110) films had in-plane M_r and H_c value that were intermediate of those for (001) and (110), this may simply reflect the fact that the CFO phase of the nanostructure for (110) did not spread-out as much as that for (001), and also was not as well dimensionally interconnected along the in-plane direction as that for (111).

In general, the FM properties of BFO-CFO nanocomposite thin films were strongly dependent on the nanostructures of the CFO phase. The more dimensionally interconnected the CFO nanostructures were, the more the M-H loops resembled that of CFO single phase layers. Correspondingly, the more dimensionally isolated the CFO nano-

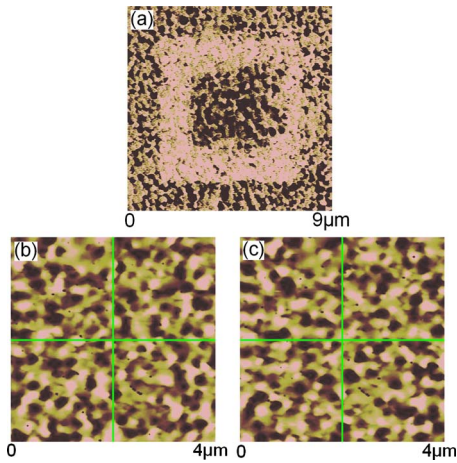


FIG. 5. (Color online) Multiferroic properties of (001) BFO-CFO nanocomposite thin films. (a) PFM images of BFO-CFO thin film after poled by $E = -10$ V applied to a $7 \times 7 \mu\text{m}^2$ and $E = +10$ V applied to a $5 \times 5 \mu\text{m}^2$ area, which demonstrate polarization rotation and MFM images of BFO-CFO thin films magnetized by (b) $H = +1$ kOe, and (c) $H = -1$ kOe applied to same regions as those in PFM image, which demonstrate spin rotation.

structures were, the more unstable the spin alignment was along that direction. For example, the CFO phase for (001) BFO-CFO was only connected in the out-of-plane direction, thus the M-H loops along that direction was similar to CFO single phase films, whereas, on (111) substrates, the CFO phase was connected in all directions, and the M-H loops for in-plane and out-of-plane directions were both similar to each other and similar to that for CFO single phase layers.

VI. MULTIFERROIC PROPERTIES, AS MEASURED BY AFM AND MAGNETIC-FORCE MICROSCOPY (MFM)

The FE and FM natures of the BFO-CFO nanocomposites were also studied by PFM and MFM, respectively. A PFM image of (001) BFO-CFO film is shown in Fig. 5(a), a $7 \times 7 \mu\text{m}^2$ square was poled by -10 V, where a $5 \times 5 \mu\text{m}^2$ area was subsequently reversely poled by $+10$ V. Switching of the polarization was evidenced by the change in contrast in the PFM images between the $5 \times 5 \mu\text{m}^2$ subarea and the layer $7 \times 7 \mu\text{m}^2$ one. This notable contrast change indicates a change in the sense of the polarization direction under E . In addition, magnetic force images of (001) films magnetized by $+1$ and -1 kOe are shown in Figs. 5(b) and 5(c), respectively. Cross lines are used to identify near-exact positions in the figures, making visual comparisons easier. On comparing these two images, some regions can be seen to be nearly opposite in contrast upon changing the sense of H . This shows that the magnetization orientation was nearly reversed between applied fields of -1 and 1 kOe. These images in Fig. 5 demonstrate the multiferroic characteristics and a local scale for our ME nanocomposites, which are similar in nature to the average ones measured by P-E and M-H hysteresis loops.

VII. ME PROPERTIES

Finally, we measured the ME coefficient as a function of ac magnetic field for the (001), (110), and (111) BFO-CFO

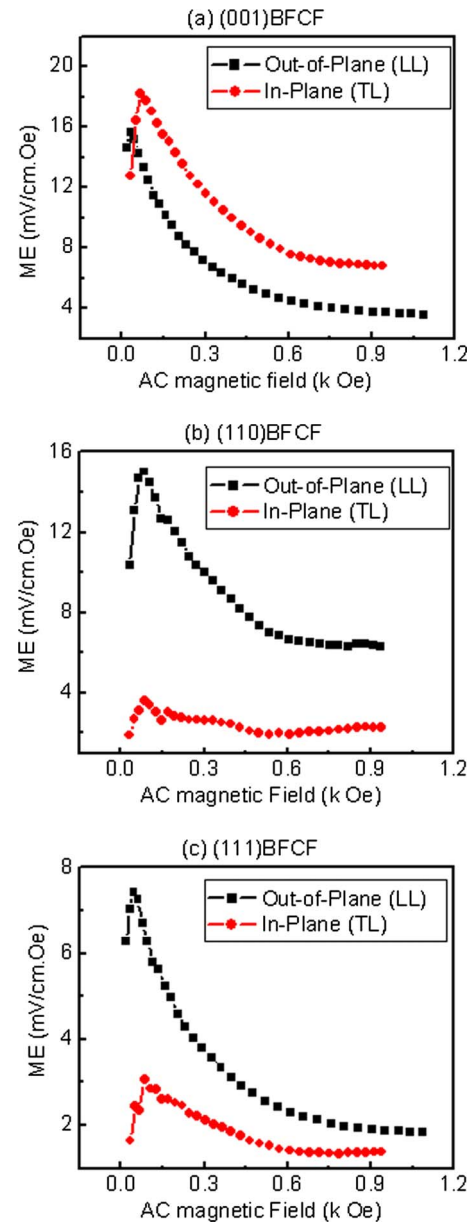


FIG. 6. (Color online) ME coefficient for (a) (001), (b) (110), and (c) (111) oriented self-assembled BFO-CFO nanocomposite thin films as a function of ac magnetic field amplitude in both out-of-plane (longitudinal-longitudinal) and in-plane (transverse-longitudinal) directions.

nanocomposite films along both in-plane and out-of-plane directions as shown in Fig. 6. Please note that the L-L mode designates a longitudinally magnetized and longitudinally poled coefficient, whereas the T-L mode designates a transversely magnetized and longitudinally poled one. The L-L and T-L mode coefficients were measured by applying an ac magnetic field along the out-of-plane and in-plane directions, respectively. In this figure, the ME coefficient can be seen to increase rapidly with increase in ac magnetic field, reaching a maximum value near $H_{ac} \approx 100$ Oe, and the decreasing gradually with further increase of H_{ac} .

For (110) and (111) films, the ME coefficients for the out-of-plane direction were about three to four times higher than those in-plane, this is similar in trend to that between L-L and T-L modes for bulk ME composites, as previously

reported.⁹ In the case of the L-L mode, the magnetostriction strain of the CFO phase is oriented along the longitudinal direction. Due to elastic coupling at the interphase interfaces, this strain is then transferred to the FE phase, which in turn generates a voltage, via the piezoelectric d_{33} coefficient, along the longitudinal direction. For the T-L mode, the magnetostriction strain of the CFO phase is oriented along the transverse direction, which is elastically coupled at the interphase interfaces to BFO, generated a voltage via d_{31} . Since $d_{31} < d_{33}$, the ME voltage for the T-L mode is notably less than that of the L-L.

However, for (001) films, the ME coefficients in the T-L mode were slightly higher than that for L-L—an anomalous result for the anisotropy of the ME tensor coefficients. The origin of this anomaly is not certain at this time. We could conjecture that this anomalous ME behavior may reflect an asymmetric magnetic behavior for (001) BFO–CFO films (see Fig. 4), where H_c for the in-plane direction was only half that for the out-of-plane one. Consequently, the magnetization of (001) CFO might rotate more easily along the in-plane direction than it can for the other orientations of CFO thin films. If that were the case, the effective linear magnetostrictive coefficient for CFO nanopillars along the in-plane direction might be appreciably enhanced.

In general, the maximum value of the ME coefficient for the L-L mode of BFO–CFO films follows the trend of $ME_{(001)} > ME_{(110)} > ME_{(111)}$ (16, 15, and 8 mV/cm Oe). The underlying reason may be simply that the longitudinal piezoelectric d_{33} coefficient of the BFO phase of the BFO–CFO films follows the trends of $d_{33(001)} > d_{33(110)} > d_{33(111)}$. Another contributing reason maybe the fact that the constraint stress imposed by the substrates follows the trend of $\sigma_{(111)} > \sigma_{(110)} > \sigma_{(001)}$. Accordingly, the constraint stress for the CFO nanopillars on (001) STO substrates may be less than that for a CFO matrix phase on (111) STO.

VIII. SUMMARY

The FE, FM, and ME properties of (001), (110), and (111) two-phase BFO–CFO nanostructured thin films were studied. Our results demonstrate that (i) the FE properties are similar to that of single phase BFO, following a trend of $P_{(111)} > P_{(110)} > P_{(001)}$, (ii) the FM properties depend on the nanostructure of the CFO phase, with a difference between in-plane and out-of plane directions that follows a trend of $(001) > (110) > (111)$, and (iii) the ME properties depend on the combined effects of FE/FM properties and the nanostructure, where the ME coefficient follows a trend of $ME_{(001)} > ME_{(110)} > ME_{(111)}$.

ACKNOWLEDGMENTS

We gratefully acknowledge financial support from the U.S. Department of Energy under Contract No. DE.-AC02-98CH10886 and the Office of the Air-Force Office of Scien-

tific Research under Grant No. FA 9550-06-1-0410.

- ¹P. Curie, J. Phys. **3**, 393 (1894).
- ²I. E. Dzyaloshinskii, Zh. Eksp. Teor. Fiz. **37**, 881 (1959).
- ³D. N. Astrov, Zh. Eksp. Teor. Fiz. **11**, 708 (1960).
- ⁴G. T. Rado and V. J. Folen, Phys. Rev. Lett. **7**, 310 (1961).
- ⁵J. Ryu, A. V. Carazo, K. Uchino, and H. E. Kim, Jpn. J. Appl. Phys., Part **1** **40**, 4948 (2001).
- ⁶J. Ryu, S. Priya, K. Uchino, and H. E. Kim, J. Electroceram. **8**, 107 (2002).
- ⁷C. W. Nan, Phys. Rev. B **50**, 6082 (1994).
- ⁸S. X. Dong, J. F. Li, and D. Viehland, Appl. Phys. Lett. **83**, 2265 (2003).
- ⁹S. X. Dong, J. F. Li, and D. Viehland, IEEE Trans. Ultrason. Ferroelectr. Freq. Control **50**, 1253 (2003).
- ¹⁰S. X. Dong, J. R. Cheng, J. F. Li, and D. Viehland, Appl. Phys. Lett. **83**, 4812 (2003).
- ¹¹K. S. Chang, M. A. Aronova, C. L. Lin, M. Murakami, M. H. Yu, J. Hattrick-Simpers, O. O. Famodu, S. Y. Lee, R. Ramesh, M. Wuttig, I. Takeuchi, C. Gao, and L. A. Bendersky, Appl. Phys. Lett. **84**, 3091 (2004).
- ¹²M. Murakami, K. S. Chang, M. A. Aronova, C. L. Lin, M. H. Yu, J. Hattrick-Simpers, M. Wuttig, I. Takeuchi, C. Gao, B. Hu, S. E. Lofland, L. A. Knauss, and L. A. Bendersky, Appl. Phys. Lett. **87**, 112901 (2005).
- ¹³M. Ziese, A. Bollero, I. Panagiotopoulos, and N. Moutis, Appl. Phys. Lett. **88**, 212502 (2006).
- ¹⁴H. C. He, J. P. Zhou, J. Wang, and C. W. Nan, Appl. Phys. Lett. **89**, 052904 (2006).
- ¹⁵J. P. Zhou, H. C. He, Z. Shi, and C. W. Nan, Appl. Phys. Lett. **88**, 013111 (2006).
- ¹⁶C. Deng, Y. Zhang, J. Ma, Y. Lin, and C. W. Nan, J. Appl. Phys. **102**, 074114 (2007).
- ¹⁷S. Ryu, J. H. Park, and H. M. Jang, Appl. Phys. Lett. **91**, 142910 (2007).
- ¹⁸H. C. He, J. Wang, J. P. Zhou, and C. W. Nan, Adv. Funct. Mater. **17**, 1333 (2007).
- ¹⁹J. G. Wan, X. W. Wang, Y. J. Wu, M. Zeng, Y. Wang, H. Jiang, W. Q. Zhou, G. H. Wang, and J. M. Liu, Appl. Phys. Lett. **86**, 122501 (2005).
- ²⁰H. Ryu, H. Murugavel, J. H. Lee, S. C. Chae, T. W. Noh, Y. S. Oh, H. J. Kim, K. H. Kim, J. H. Jang, M. Kim, C. Bae, and J. G. Park, Appl. Phys. Lett. **89**, 102907 (2006).
- ²¹J. G. Wan, H. Zhang, X. W. Wang, D. Pan, J. M. Liu, and G. Wang, Appl. Phys. Lett. **89**, 122914 (2006).
- ²²X. L. Zhong, J. B. Wang, M. Liao, G. J. Huang, S. H. Xie, Y. C. Zhou, Y. Qiao, and J. P. He, Appl. Phys. Lett. **90**, 152903 (2007).
- ²³M. Liu, X. Li, J. Lou, S. Zheng, K. Du, and N. X. Sun, J. Appl. Phys. **102**, 083911 (2007).
- ²⁴H. Zheng, J. Wang, S. E. Lofland, Z. Ma, L. Mohaddes-Ardabili, T. Zhao, L. Salamanca-Riba, S. R. Shinde, S. B. Ogale, F. Bai, D. Viehland, Y. Jia, D. G. Gchlom, M. Wuttig, A. Roytburd, and R. Ramesh, Science **303**, 661 (2004).
- ²⁵H. Zheng, F. Straub, Q. Zhan, P. L. Yang, W. K. Hsieh, F. Zavaliche, Y. H. Chu, U. Dahmen, and R. Ramesh, Adv. Mater. **18**, 2747 (2006).
- ²⁶H. Zheng, Q. Zhan, F. Zavaliche, M. Sherburne, F. Straub, M. O. Cruz, L. Q. Chen, U. Dahmen, and R. Ramesh, Nano Lett. **6**, 1401 (2006).
- ²⁷C. W. Nan, G. Liu, and Y. Lin, Phys. Rev. Lett. **94**, 197203 (2005).
- ²⁸L. Yan, Z. P. Xing, Z. G. Wang, T. Wang, G. Y. Lie, J. F. Li, and D. Viehland, Appl. Phys. Lett. **94**, 192902 (2009).
- ²⁹K. Y. Yun, M. Noda, M. Okuyama, H. Seaki, H. Tabata, and K. Saito, J. Appl. Phys. **96**, 3399 (2004).
- ³⁰M. Soliman Selim, G. Turky, M. A. Shouman, and G. A. El-Shobaky, Solid State Ionics **120**, 173 (1999).
- ³¹J. L. Wang, Ph.D. thesis, University of Maryland, 2005.
- ³²Y. C. Wang, J. Ding, J. B. Yi, B. H. Liu, T. Yu, and Z. X. Shen, Appl. Phys. Lett. **84**, 2596 (2004).
- ³³P. C. Dorsey, P. Lubitz, D. B. Chrisey, and J. S. Horwitz, J. Appl. Phys. **79**, 6338 (1996).
- ³⁴Y. Suzuki, R. B. van Dover, E. M. Gyorgy, J. M. Phillips, V. Korenivski, D. J. Werder, C. H. Chen, R. J. Cava, J. J. Krajewski, W. F. Peck, Jr., and K. B. Bo, Appl. Phys. Lett. **68**, 714 (1996).
- ³⁵Y. Suzuki, Annu. Rev. Mater. Res. **31**, 265 (2001).